

Multi-beam single-photon-counting three-dimensional imaging lidar

ZHAOHUI LI,¹ E WU,¹ CHENGKAI PANG,¹ BINGCHENG DU,¹ YULIANG TAO,²
HUAN PENG,² HEPING ZENG,^{1,4} AND GUANG WU^{1,3,*}

¹State Key Laboratory of Precision Spectroscopy, East China Normal University, Shanghai 200062, China

²Beijing Institute of Space Mechanics & Electricity, Beijing 10009, China

³Collaborative Innovation Center of Extreme Optics, Shanxi University, Taiyuan, Shanxi 030006, China

⁴hpzeng@phy.ecnu.edu.cn

*gwu@phy.ecnu.edu.cn

Abstract: Photon-counting laser ranging has attracted a lot of research interest for its application in the altimeter. In this letter, we report a large scale multi-beam photon-counting laser imaging system by using 100 laser beams in linear array as the light source. Taking advantage of a 100-channel low-noise high-efficiency single-photon detector, the three-dimensional image of remote targets could be constructed rapidly according to the time-of-flight measurement. This system provides a solution for a high-speed, high-resolution, low energy-consumption pushbroom airborne or spaceborne laser altimeter.

© 2017 Optical Society of America

OCIS codes: (030.5260) Photon counting; (110.6880) Three-dimensional image acquisition; (280.3640) Lidar.

References and links

1. H. Zwally, B. Schutz, W. Abdalati, J. Abshire, C. Bentley, A. Brenner, J. Bufton, J. Dezio, D. Hancock, D. Harding, T. Herring, B. Minster, K. Quinn, S. Palm, J. Spinhrne, and R. Thomas, "ICESat's laser measurements of polar ice, atmosphere, ocean, and land," *J. Geodyn.* **34**(3-4), 405–445 (2002).
2. A. McCarthy, R. J. Collins, N. J. Krichel, V. Fernández, A. M. Wallace, and G. S. Buller, "Long-range time-of-flight scanning sensor based on high-speed time-correlated single-photon counting," *Appl. Opt.* **48**(32), 6241–6251 (2009).
3. S. Bellisai, D. Bronzi, F. A. Villa, S. Tisa, A. Tosi, and F. Zappa, "Single-photon pulsed-light indirect time-of-flight 3D ranging," *Opt. Express* **21**(4), 5086–5098 (2013).
4. C. L. Glennie, W. E. Carter, R. L. Shrestha, and W. E. Dietrich, "Geodetic imaging with airborne LiDAR: the Earth's surface revealed," *Rep. Prog. Phys.* **76**(8), 086801 (2013).
5. A. McCarthy, X. Ren, A. Della Frera, N. R. Gemmill, N. J. Krichel, C. Scarcella, A. Ruggeri, A. Tosi, and G. S. Buller, "Kilometer-range depth imaging at 1,550 nm wavelength using an InGaAs/InP single-photon avalanche diode detector," *Opt. Express* **21**(19), 22098–22113 (2013).
6. H. Zhou, Y. He, L. You, S. Chen, W. Zhang, J. Wu, Z. Wang, and X. Xie, "Few-photon imaging at 1550 nm using a low-timing-jitter superconducting nanowire single-photon detector," *Opt. Express* **23**(11), 14603–14611 (2015).
7. A. Swatantran, H. Tang, T. Barrett, P. DeCola, and R. Dubayah, "Rapid, High-Resolution Forest Structure and Terrain Mapping over Large Areas using Single Photon Lidar," *Sci. Rep.* **6**(1), 28277 (2016).
8. H. Araki, S. Tazawa, H. Noda, Y. Ishihara, S. Goossens, S. Sasaki, N. Kawano, I. Kamiya, H. Otake, J. Oberst, and C. Shum, "Lunar global shape and polar topography derived from Kaguya-LALT laser altimetry," *Science* **323**(5916), 897–900 (2009).
9. P. Tarolli, "High-resolution topography for understanding Earth surface processes: opportunities and challenges," *Geomorphology* **216**, 295–312 (2014).
10. J. Ping, Q. Huang, J. Yan, J. Cao, G. Tang, and R. Shu, "Lunar topographic model CLTM-s01 from Chang'E-1 laser altimeter," *Sci. China Ser. G.* **52**(7), 1105–1114 (2009).
11. D. E. Smith, M. T. Zuber, G. B. Jackson, J. F. Cavanaugh, G. A. Neumann, H. Riris, X. Sun, R. S. Zellar, C. Coltharp, J. Connelly, R. B. Katz, I. Kleynner, P. Liiva, A. Matuszeski, E. M. Mazarico, J. F. McGarry, A.-M. Novo-Gradac, M. N. Ott, C. Peters, L. A. Ramos-Izquierdo, L. Ramsey, D. D. Rowlands, S. Schmidt, V. S. Scott, G. B. Shaw, J. C. Smith, J.-P. Swinski, M. H. Torrence, G. Unger, A. W. Yu, and T. W. Zagwodzki, "The lunar orbiter laser altimeter investigation on the lunar reconnaissance orbiter mission," *Space Sci. Rev.* **150**(1-4), 209–241 (2010).

12. M. S. Moussavi, W. Abdalati, T. Scambos, and A. Neuenschwander, "Applicability of an automatic surface detection approach to micro-pulse photon-counting lidar altimetry data: implications for canopy height retrieval from future ICESat-2 data," *Int. J. Remote Sens.* **35**(13), 5263–5279 (2014).
13. J. S. Deems, T. H. Painter, and D. C. Finnegan, "Lidar measurement of snow depth: a review," *J. Glaciol.* **59**(215), 467–479 (2013).
14. W. Becker, *Advanced Time-Correlated Single Photon Counting Techniques* (Springer-Verlag, 2005).
15. M. Ren, X. Gu, Y. Liang, W. Kong, E. Wu, G. Wu, and H. Zeng, "Laser ranging at 1550 nm with 1-GHz sine-wave gated InGaAs/InP APD single-photon detector," *Opt. Express* **19**(14), 13497–13502 (2011).
16. A. McCarthy, N. J. Krichel, N. R. Gemmell, X. Ren, M. G. Tanner, S. N. Dorenbos, V. Zwiller, R. H. Hadfield, and G. S. Buller, "Kilometer-range, high resolution depth imaging via 1560 nm wavelength single-photon detection," *Opt. Express* **21**(7), 8904–8915 (2013).
17. Z. Bao, Y. Liang, Z. Wang, Z. Li, E. Wu, G. Wu, and H. Zeng, "Laser ranging at few-photon level by photon-number-resolving detection," *Appl. Opt.* **53**(18), 3908–3912 (2014).
18. Y. Liang, J. Huang, M. Ren, B. Feng, X. Chen, E. Wu, G. Wu, and H. Zeng, "1550-nm time-of-flight ranging system employing laser with multiple repetition rates for reducing the range ambiguity," *Opt. Express* **22**(4), 4662–4670 (2014).
19. A. Maccarone, A. McCarthy, X. Ren, R. E. Warburton, A. M. Wallace, J. Moffat, Y. Petillot, and G. S. Buller, "Underwater depth imaging using time-correlated single-photon counting," *Opt. Express* **23**(26), 33911–33926 (2015).
20. A. Yu, M. Krainak, D. Harding, J. Abshire, X. Sun, S. Valett, J. Cavanaugh, and L. Ramos-Izquierdo, "Spaceborne laser instruments for high-resolution mapping," *Proc. SPIE* **7578**, 757802 (2010).
21. NASA, "Our Mission | ICESat-2," <http://icesat-2.gsfc.nasa.gov/mission>.
22. A. Yu, M. Stephen, S. X. Li, G. B. Shaw, A. Seas, E. Dowdye, E. Troupaki, P. Liiva, D. Poullos, and K. Mascetti, "Space laser transmitter development for ICESat-2 Mission," *Proc. SPIE* **7578**, 757809 (2010).
23. D. Harding, P. Dabney, J. Abshire, T. Huss, G. Jodor, R. Machan, J. Marzouk, K. Rush, A. Seas, C. Shuman, X. Sun, S. Valett, A. Vasilyev, A. Yu, and Y. Zheng, "The slope imaging multi-polarization photon-counting Lidar: an advanced technology airborne laser altimeter," *NASA Earth Science Technology Forum* **10**, 253–256 (2010).
24. S. Pellegrini, G. S. Buller, J. M. Smith, A. M. Wallace, and S. Cova, "Laser-based distance measurement using picosecond resolution time-correlated single-photon counting," *Meas. Sci. Technol.* **11**(6), 712–716 (2000).

1. Introduction

Remote laser detection and ranging (lidar) shows considerable significance with applications in geography, forestry, atmospheric physics due to the advantages of small volume and high precision [1–6]. Thereinto, the spaceborne lidar has been widely used as laser altimeter to study the global topography [7–11], the ice sheet altimeter [1], the canopy height [7] and so on. However, most laser altimeters focus on only one ground point at a time, which could not achieve dense point cloud data quickly. To reduce the time for globally mapping the surface topography, the Lunar Orbiter Laser Altimeter (LOLA) used a five-beam scheme without scanning, which also enabled surface-slope measurement [8]. With more laser beams in use, the topography would get higher resolution [9]. However, a large number of laser beams would consume too much energy for the spaceborne platform with the traditional linear optical detection. Photon-counting laser ranging and imaging deeply decrease the power consumption for long-distance measurement by improving the detecting sensitivity to quantum limit with techniques of single-photon detection and time-correlation single-photon counting (TCSPC) [12–19]. Based on the single-photon counting technique, a spaceborne lidar Surface Topography (LIST) scheme was proposed in Ref [20]. It was aiming to map the global topography and the vegetation structure quickly with high resolution and wide swath width. The three-dimensional (3D) topographic imaging was constructed by combining the swath mapping technique with a multi-laser-beam linear array and a photon-counting detector array of 1000 pixels. In this scheme, the light source was from 10 laser beams, and each beam was divided into 100 beams by a diffractive optical element (DOE) beam-divider. And, the weak reflected light was detected by the detector array at nearly single-photon sensitivity. To realize the multi-beam photon-counting lidar of LIST, a micro-pulse photon-counting lidar system, named ATLAS was planned to launch in the ICESat-2 mission of NASA [21, 22]. ATLAS was planned to use 6 laser beams with a multi-channel single-photon detector. NASA developed an airborne slope imaging multi-polarization photon-counting lidar (SIMPL) to demonstrate photon-counting laser altimetry method for high-

resolution, swath mapping of topography and surface properties from space [23]. The SIMPL consisted of 4 laser beams, and each beam contained two wavelengths of 532 nm and 1064 nm. At the receiver, a 16-channel Si-avalanche photodiode (Si-APD) single-photon detector was used to detect the orthogonal polarizations of each beam at different wavelengths. But, the number of the laser beams in these multi-beam photon-counting lidars was less than 10, which was far from the LIST.

In this paper, we demonstrated a multi-beam photon-counting 3D lidar system, which was a 1:10 miniature demonstration of LIST. A 532-nm sub-nanosecond pulse laser was divided to 100 beams in a linear array with a DOE. And a 100-channel Si-APD single-photon detector was applied to realize 100-beam photon-counting ranging and scanning imaging. The system shows several striking features. Firstly, since 100 laser beams were used with 100 detection channels, the swath width is much larger, leading to a short acquisition time for the 3D image. Secondly, the implementation of integrated swapping plate consisting both the transmitting and the receiving devices enhanced the stability of the system, which is suitable for the airborne or spaceborne altimeter. Most importantly, the 100-channel single-photon detector based on Si-APDs provides high detection efficiency, low noise, short time jitter and no cross talk, paving the way to a high-resolution lidar system with low energy consumption.

2. System description

Figure 1 shows the scheme of the multi-beam photon-counting 3D lidar system. The whole system was mounted on a 2D rotation stage to scan the transmitting and the receiving devices. There was no relatively moving between the two parts, functioning the same as the swath mapping technique of LIST [20]. A solid-state laser at 532 nm produced short pulses at a repetition rate of 10 kHz with a pulse energy of $\sim 0.3 \mu\text{J}/\text{pulse}$. The laser pulse duration was about 600 ps. The diameter of the laser beam spot was expanded from 4 mm to 10 mm with the divergence angle of 0.125 mrad by a beam expander, which was composed of two lens L1 and L2 as shown in Fig. 1. A very little part of the light leaked from M2 was detected by a PIN photodiode to trigger the time-of-flight measurement. Then, the laser was divided into more than 100 beams in linear array by a DOE. The divergence angle between the adjacent two beams was 0.25 mrad. With 100 beams, the swath angle was about 24.75 mrad.

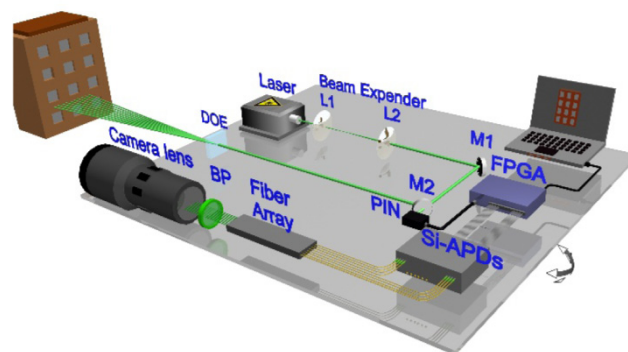


Fig. 1. Schematic of the multi-beam photon-counting lidar system. Pulsed laser source: 532-nm with repetition rate of 10 kHz and pulse duration of 600 ps. Beam expander: composed of two lens L1 ($f = 3.3 \text{ mm}$) and L2 ($f = 60 \text{ mm}$). M1, M2: high reflection mirror at 532 nm. PIN: fast photodiode. DOE: diffractive optical element to produce 100 beams with divergence angle of 0.25 mrad between adjacent beams. Camera Lens: long-focal-length adjustable camera lens. BP: bandpass filter at 532 nm with linewidth of 1.0 nm. Fiber array: composed of 100 multimode fibers. Si-APDs: 100 Si-APDs with fiber pigtail on heat sinks. FPGA: seven FPGA board integrated in one box for data processing.

Figure 2(a) shows the photo of the laser spot array on the wall of a building 600-m away taken by a camera with 10 seconds exposure time at night. The laser power was concentrated on the central 100 beams. And among the 100 beams, the intensity of the central one was 10 times higher than the others. The diameter of the central spot was about 90 mm on the wall while the others were about 60 mm. The distance between adjacent spots was about 0.15 m on average on the wall. Therefore, the swath width was about 14.85 m.

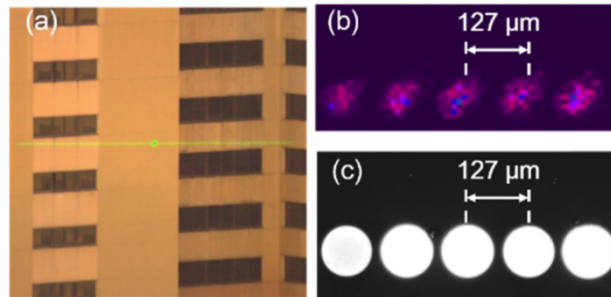


Fig. 2. (a) Laser beam spots on the wall of the target building 600 m away, (b) beam spot at the focus of the camera lens taken by a CCD camera, and (c) microscope image of the multi-mode fiber array facet.

The reflected light was collected by a long-focal-length adjustable camera lens (Tamron, A011 SP 150-600 mm f/5-6.3 Di VC USD). The focal-length was adjusted to about 508 mm. The diameter of the effective aperture was 95 mm. A narrow bandpass (BP) filter with 1-nm bandwidth at 532 nm was used to remove the stray light noise. We firstly checked the beam profile with a beam analyzer CCD at the focus of the camera lens as shown in Fig. 2(b) by illuminating a white board 30-m away. By slightly adjusting the focal length of the camera lens, we could obtain a distance between two adjacent beam spots as 127 μm at the focus to match the multi-mode fiber array. Then, the CCD was replaced by a fiber array. The reflected photons were focused into the linear fiber array. The diameter of the fiber core was 105 μm, and the distance between the fiber cores was 127 μm as shown in Fig. 2(c). At the end of each fiber, a single-photon counting module based on Si-APD was connected. In this way, the collected photons were detected by the 100-channel single-photon detector. The total efficiency of system was about 20% including the transmittance of the camera lens and the bandpass filter, the coupling efficiency of the fiber array, and the detection efficiency of the single-photon detector. The outputs of the single-photon detectors and the synchronization signal of the laser source were recorded by a 100-channel time-to-digital converter (TDC) which was formed of seven field programmable gate array (FPGA) boards. The minimum time bin width of the TDCs was 64 ps. The synchronization laser pulse signal from the PIN photodiode was connected to the START channel of the TDC while the outputs from the single-photon detectors were connected to 100 STOP channels, respectively. The TDC would provide a digital representation of the time between the START channel and the STOP channels which is the so-called time-of-flight measurement. The time bin width of the TDC was adjusted according to the ranging distance. A computer collected the photon arrival information from the TDC via a USB cable, and also controlled the 2D rotation stage to scan.

We carried out an experiment to estimate the optical cross talk between the pixels of the fiber array. In the experiment, an LED array (1×16) at 532 nm was used as the light source. The receiving device was placed 30-m away from the LED. The light was collected and formed 16 focusing spots in a line. The focusing spots were coupled into 16 adjacent fibers among the 100-fiber array. By switching on only one of the LED pixel each time, we measured the optical power at the output of the corresponding fiber together with those at the neighbor fibers. The ratio of the two was regarded as the optical cross talk of the system. In

the experiment, the optical cross talk between the fiber channels was measured to be less than 1%.

A homebuilt 100-channel single-photon detector was used to detect the signal from the fiber array. The photons were coupled to the Si-APD (SAP500, LASER COMPONENTS) with a fiber pigtail of 105 μm in diameter. The diameter of the Si-APD's sensitive detection area was about 500 μm . And all the 100 Si-APDs were operated in Geiger-mode on seven heat sinks with Peltier cooling to -10°C . They were actively quenched and reset individually and produced 100 independent outputs. The quench and reset signals were generated from the FPGA boards. The detection efficiency and dark counts of the 100 Si-APDs were plotted in Fig. 3(a). The average detection efficiency was about 36.8%. According to the statistics on the detection efficiency in Fig. 3(b), among all the 100 Si-APDs, there were 95 channels with a detection efficiency higher than 30%. And the maximum detection efficiency could reach 71%. As shown in Fig. 3(c), most of them were operated at low dark counts noise less than the average value of 3×10^3 counts per second (cps). The variance between different channels on the detection efficiency and dark counts noise was mainly due to the coupling of the fiber pigtails. Since the 100 single-photon counting modules operated independently, there was no cross talk noise between different channels, reducing the error counts in the acquisition.

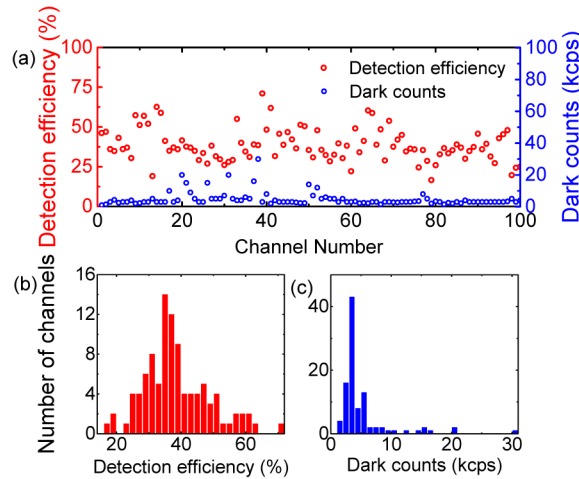


Fig. 3. (a) Detection efficiency and dark counts of the 100 Si-APD channels. The calibration of each channel was carried out with an attenuated pulsed laser independently. The operation temperature was set at -10°C , (b) statistics on the detection efficiency. Binning size: 1%, and (c) statistics on the dark counts. Binning size: 0.5 kcps.

3. Experiment and result

The time jitter of each Si-APD channel was measured individually with a short-pulse laser and a time-correlation single-photon counter (TCSPC, HydraHarp 400, PicoQuant) to be 800 ps. The TDC time bin width was set at 64 ps for the time-of-flight measurement. Considering the pulse duration of the laser source, the time jitter of the detectors and the TDC time bin width, the total time jitter of the lidar system was about 1 ns on average according to

$$\Delta t = \sqrt{t_L^2 + t_{PIN}^2 + t_D^2 + t_{TDC}^2}. \quad (1)$$

Where t_L is the pulse duration of the laser source (~ 600 ps), t_{PIN} is the time jitter of the PIN photodiode (< 10 ps), t_D is the time jitter of the detector (~ 800 ps), and t_{TDC} is the time bin width of the TDC (64 ps).

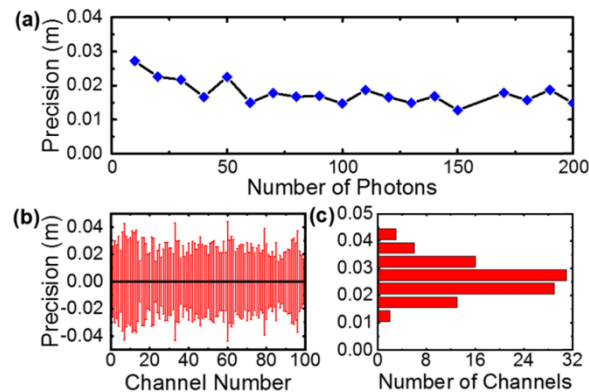


Fig. 4. (a) Precision of the single channel photon-counting laser ranging as a function of photon counts, (b) precision of the 100 channels measured when the detected photon number was 65, (c) statistics on the precision data in (b).

Assuming Poissonian statistics for the data in the measurements, the precision of the photon-counting laser ranging was inversely proportional to \sqrt{n} , where n is the photon counts [24]. We measured the depth precision of the single channel photon-counting laser ranging with different photon counts as shown in Fig. 4(a). The precision of lidar system was about 27 mm with 10 photon counts. With more detected photons, the precision got higher and higher but tended to a constant with large photon numbers. Since the counting rate of the reflected photons was quite low, balancing the precision against the acquisition time, we set the detected photon number to be around 65 for the ranging, resulting in a precision to be about 20 mm. And the precision improved very limited, as the photon counts continued to rise. Targeting at a flat board, we estimated the depth precision of the whole lidar system with 100 channels. We repeated the measurements for 100 times on the same target with 65 detected photons on each channel. The standard deviation of the average peak value was regarded as the depth precision of the lidar system as shown in Fig. 4(b). The statistics in Fig. 4(c) indicates that the precision of the 100 channels was mainly at 25 mm. The average precision was about 26 mm.

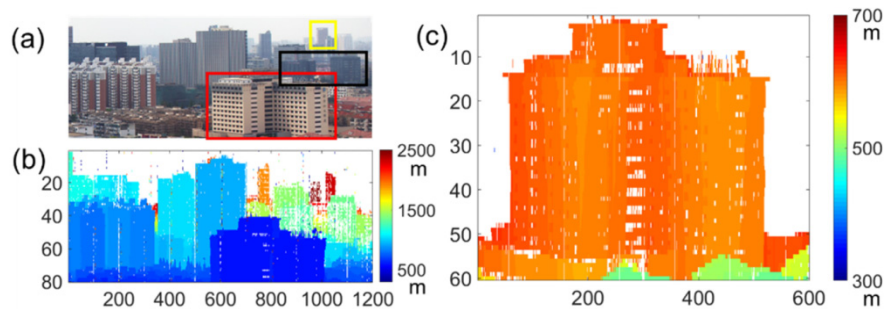


Fig. 5. (a) Real photo of the target buildings, (b) rebuilt lidar image of the buildings in vision, and (c) detailed lidar image of the target building in the red box in (a).

Figure 5 shows the image acquired by the multi-beam photon-counting lidar system with comparison of the real photo of the building. Figure 5(a) is the real photo taken in day time. Buildings at different distance could be seen clearly for comparison. Figures 5(b) and 5(c) are images acquired by the multi-beam photon-counting lidar system in a clear evening (at 20:30 local time) in July (Sunset at 18:58 local time) in Shanghai. The visibility was reported to be 9.7 km. The road lightings and landscape lightings caused a background noise of about 6

keeps on each Si-APD channel. In the system, the 100-channel array was employed horizontally in one line and the system worked in the line-by-line scanning mode. The scanning resolution of the rotational plate was set at 25 mrad/point in horizontal direction, corresponding to a spatial resolution of 0.25 mrad/channel. In the vertical direction, the scanning resolution was set at 1.67 mrad/point. Figure 5(b) shows the image of 80×12 acquisitions (80×1200 pixels). In the vertical direction, the motor scanned 133.6 mrad in 80 steps. And in the horizontal direction, the motor scanned 300 mrad in 12 steps. Therefore, the resolution of each frame is $80 \times (12 \times 100)$. The color bar scales refer to the real distance of the buildings from the lidar system. The accumulation time for the scan was set at 1 s/line. The average signal photon counts of each single-photon detecting channel was about 65 cps. The whole acquisition time for such an image cost about 20 min. Almost all the tall buildings in the real photo could be rebuilt in the image. The farthest building in the image was about 2400 m away marked with a yellow box in the real photo, indicating the ranging distance limit of the system with such resolution. Notice that, there were two buildings with black outer walls in the vision marked with a black box in the real photo. Though the reflection of these two buildings was much lower than the others due to the color, they could also be recognized in the rebuilt image owing to the sensitive detection of the returning photons. Thanks to the high detection efficiency of the single-photon detector, the output energy of the laser source could be lowered, suitable for a low-energy consumption lidar system. A bright line appeared periodically in the image. That was caused by one of the Si-APD channels of high dark counts noise. However, according to this dark line by this “bad” channel, we could approximately verify if the rebuilt image was correct. Since the 100 single-photon counting modules operated independently, it would not cause too much change by replacing any “bad” channel in the detection part of the system without disturbing other channels.

The yellow building in the red box in Fig. 5(a) is about 600 m away. We changed the TDC time bin width to 128 ps to perform a zoomed-in image. The detailed image is shown in Fig. 5(c). The windows of the building could be recognized clearly in the image due to lack of collected photons from the dark brown glass windows. And the corner of the building could be identified by the distance difference.

The demonstration shows that the stability of the multi-beam lidar system with 100 laser beams and 100 single-photon detector channels enables the large-area field swath with high speed for the 3D image. As the average counting rate of the detected photons on each single-photon detector was about 0.0065/pulse in this experiment, the system acquired 10^4 pulses to accumulate about 65 photon counts of each channel, leading to a precision of ~ 20 mm. If the detected photon-counting rate increased to 0.65/pulse, and the acquisition time could be reduced to be 10 ms/line containing 100 pixels while keeping the same precision. Thus, it will take only 9.6 seconds to get a 3D picture of 80×1200 pixels, excluding the time of rotators controlling and data transmission.

4. Conclusion

In conclusion, we realized a multi-beam photon-counting lidar system with 100 beams and a 100-channel Si-APD single-photon detector. The striking features of the system such as high speed, high stability, and high resolution make it suitable for a low-energy consumption airborne or spaceborne altimeter.

Funding

National Key R&D Program of China (2016YFB0400904); National Natural Science Foundation of China (11621404, 11374105, and 61378033); Program of Introducing Talents of Discipline to Universities (B12024); Shanghai International Cooperation Project (16520710600); and Shuguang Program (15SG22).